Modeling of Casting, Welding, and Advanced Solidification Processes - XII
Edited by: Steve L. Cockcroft and Daan M. Maijer
TMS (The Minerals, Metals & Materials Society), 2009

MODELING AND IN-SITU X-RAY VIDEO MICROSCOPY OF CONFINED EQUIAXED GRAIN GROWTH AND BUOYANT MOTION IN AL-CU

Pierre Delaleau[1], Ragnvald H. Mathiesen[2] , Paul L. Schaffer[1], Lars Arnberg[1], Christoph Beckermann[3]

[1]Department of Materials Science and Engineering;
NTNU, N-7491 Trondheim, Norway
[2]Department of Physics;
NTNU, N-7491 Trondheim, Norway
[3]Department of Mechanical and Industrial Engineering;
The University of Iowa, IA 52242, U.S.A.

Keywords: Equiaxed grains, Buoyancy, Synchrotron radiation, Solidification, Aluminium alloys.

Abstract

Equiaxed dendritic growth in grain refined Al-x wt% Cu (x=15-25) has been studied in-situ during directional solidification by means of synchrotron X-ray video microscopy. At these compositions, the α-Al grains have a lower density than the surrounding melt and experience buoyant forces which affect their growth rates and morphologies. As the samples are concealed within a thin container, the walls severely influence grain motion. A model for one single grain has been derived taking into account the influence of sample confinement on the drag force exerted on the free grain. The model is compared with the in-situ experiments to evaluate its present merits and to devise possible routes for further improvement in order to develop it to describe α-Al dendritic growth during buoyant motion.

Introduction

The microstructure determines the mechanical properties of a casting, and chemical inhomogeneities that arise during processing can result in serious defects. Accordingly, understanding, modeling, and controlling the various physical phenomena that occur during liquid to solid transformation are core issues in applied and fundamental solidification science. Generally, solidification may lead to two types of dendritic grain morphologies: columnar and equiaxed. In Al-based alloys where inoculation can be promoted with the addition of TiB_2 particles to the melt, equiaxed dendritic growth is the prevalent mode for primary phase formation. The governing phenomena are dynamical and, as a consequence, it is of major interest to investigate solidification processing in-situ and in real time. Several of the Al-based alloys are excellent candidates for in-situ X-radiographic investigations of solidification microstructure evolution and such experiments have been carried out previously to understand the growth of equiaxed dendritic grains [1-3]. The results presented in this paper will focus on detailed measurements and analysis of the buoyant motion and growth of equiaxed grains with different alloy compositions.

Experiments

Experimental setup

The X-ray imaging experiments were performed in-situ during directional solidification in a Bridgman furnace. A thin alloy sample was placed in the gap between the two furnace compartments and moved towards the cold stage at constant velocity by a stepping motor. The experiments were carried out at beamlines BM05 and ID22 at the European Synchrotron Radiation Facility (ESRF) using incident beams monochromatized to 15 KeV. With the employed settings, the detector system provided a field of view of approximately 1.4 x 1.4 10^{-6} m^2, and nominal temporal and spatial resolutions at ID22 of 0.15 s and 1.5 10^{-6}m, respectively, and at BM05 0.25 s and 3 10^{-6}m, respectively. A more detailed description of the experimental setup together with an introduction to the basic principles of high-energy synchrotron X-ray imaging can be found elsewhere [4].

Sample preparation

Three Al-Cu alloys with nominal compositions 15, 20 and 25 wt% Cu were prepared by melting 99.999% purity Al and Cu in a resistance furnace. At a melt superheat of ~100 K, Al-5wt%Ti-1%B grain refiner was added while stirring the melt for one minute to obtain a well-mixed nominal composition of 0.0025 wt% Ti. The alloys were then cast into a bottom chilled mould. A region free of porosity located 1 10^{-2}m from the chill was cut into rectangular slices measuring 1.1 x 2.2 $10^{-4}m^2$. The slices were polished down to thicknesses of 1.40-1.60 10^{-4}m in MA400 (BM5 experiment) and 1.95-2.05 10^{-4}m in ME599 (ID22 experiment), and coated with Boron-Nitride, before being concealed into a container made by melting together two rectangular 1.50 10^{-4}m thick quartz glass plates around the metal sheet.

In-situ experiments

For each alloy composition, multiple data sequences were collected with a systematic variation of solidification conditions. For the sequences used in the present analysis (Table I), the top furnace temperature, T_t, and the bottom furnace temperature, T_b, were independently controlled and operated with $T_b > T_t$, yielding an imposed temperature gradient, $|G|$ parallel to g, by varying T_t, T_b and the distance between the two furnaces. The sample pulling velocity, U_{sp}, was also adjusted to produce cooling rates, $dT/dt = G * U_{sp}$.

Table I. Number of sequences with the data ranges applied

Alloys	Number of samples	U_{sp} range ($10^{-6}ms^{-1}$)	G range ($10^{3}Km^{-1}$)	dT/dt range ($10^{-2}Ks^{-1}$)
Al-15wt%Cu	2	20-25	3-10	7-24
Al-20wt%Cu	3	7-23	12-16	8-36
Al-25wt%Cu	2	7-25	9-10	7-23

Post experimental data processing included flat fielding to correct the raw images for incident beam inhomogenities, followed by a binarisation, separating the fully liquid from the solid containing regions of the projection images. From the binary images, dendrite morphologies, grain sizes and local growth velocities were obtained within the accuracy provided by the spatial and temporal resolution limits.

Model description

In the image sequences, grains were observed to nucleate on both the container wall and freely in the melt. However, this study will only focus on the grains which nucleate freely in the melt and grow under buoyant and convective conditions.
Nucleation temperatures were determined for each grain when it first appeared in the image sequence as a function of location within the sample. It was assumed that the nucleated grains attained their initial size by thermally restricted growth only, with a homogeneous composition as given by the phase diagram at the nucleation temperature. As a first approach, the free equiaxed grains ahead of the coherent network in the image sequences were modeled as spheres with a radius R, deduced from the area equivalent to that of the free grains. In addition to size, $R(t)$, each grain was positioned in its centre of gravity as calculated from the binary image area.

Diffusive growth under buoyant movement
The grain growth can be approximated by the equation given by Thomas and Whelan [5]

$$\frac{dR^2}{dt} = kD \tag{1}$$

where R is the grain radius depending on the diffusion coefficient, D, the coefficient, $k=2(C_l - C_0)/(C_l - C_s)$ and time, t. For each composition, the growth average of grains which nucleate on both the container wall and freely in the melt is represented in Figure 1 and compared with the model described by equation (1) where the constant $kD = 6.3\ 10^{-4} m^2 s^{-1}$.

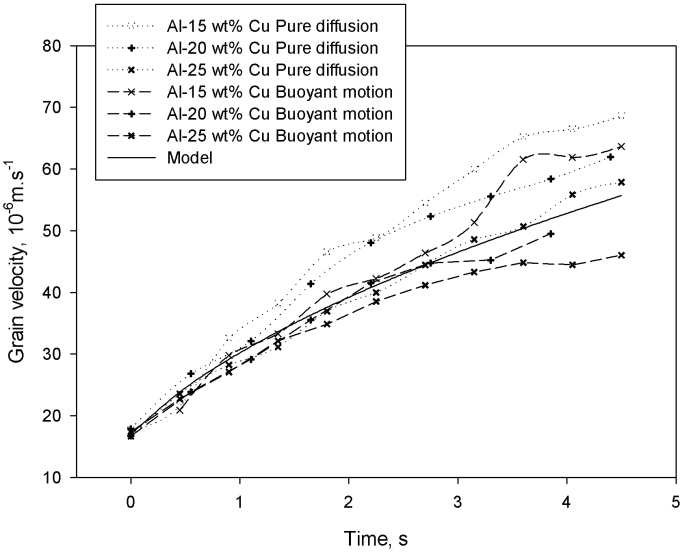

Figure 1. Grain size evolution for purely diffusive and buoyant growth for the three different compositions: 15, 20 and 25 wt% Cu and the model described by Equation (1).

The grains which nucleate on the wall container are assumed to be purely diffusive. In the early stages of their growth, the grains under buoyant motion behave like the pure diffusive case. The Peclet number is defined as $Pe=UR/D$ where U is the grain velocity, R the grain radius and D~2.5 $10^{-9}m^2s^{-1}$ the diffusion coefficient [6]. As the Peclet number is less than one, the concentration field around the grain is not affected by the motion and equation (1) remains valid under buoyant movement. However, as time increases, the growth of the grains under buoyant motion tends to be less than the purely diffusive case. As the grains are moving toward the solidification front where solute is rejected and fluid flow is changed considerably, the concentration field around the grain will also be modified and consequently its growth rate will be influenced. It is therefore necessary to determine the grain velocity and its position relative to the solidification front in order to describe how its growth will be affected. In the next section, a model is developed to calculate the grain velocity during buoyant motion depending on its size. The measured radius average will be used to compare the measured velocity average with the model.

Buoyant motion

During motion, the grain radius must remain less than sample thickness and for purely buoyant motion to be analysed only small grains in their early stages of growth can be studied. Under the growth conditions described in the previous section, the grains experience buoyant and drag forces resulting in motion in the vertical direction and the following force balance gives the equation of motion for a single isolated grain:

$$\rho_s V_s \frac{dU}{dt} = gV_s(\rho_l - \rho_s) + f(U,R) \tag{2}$$

where ρ_s and ρ_l are the solid and liquid densities respectively, R the grain radius, V_s the grain volume, U the grain velocity, g (=9.81 ms^{-2}) the gravitational acceleration and f is the drag force. A model was developed to determine the liquid and solid densities depending on the initial concentration, C_0 and the temperature field. This model is based on Scheil conditions to account for the solute transport across the solid-liquid interface and the results compare well with those obtained by Ganesan and Poirier [7]. The buoyant force can therefore be calculated knowing R at each time step. The Reynolds number is defined as $Re= 2UR/\nu$ where ν~2 $10^{-6}m^2s^{-1}$ is the kinematic viscosity of the melt [8]. For the three compositions, the maximum grain velocity was found to be ~1 $10^{-4}ms^{-1}$ and the maximum grain radius is ~5 10^{-5}m. The corresponding Reynolds number is therefore not more than 0.005, for which Stokes flow applies, yielding $f(U,R) = 6\pi\eta UR$. Moreover, inertial forces can be neglected and according to equation (2), a terminal velocity, U_t [9] is reached at each time step and is given by

$$U_t = \frac{2}{9}\frac{\left(1-\frac{\rho_s}{\rho_l}\right)gR^2}{\upsilon} \tag{3}$$

Confinement

The influence of walls on the motion of a sphere in a viscous fluid at Reynolds number considerably less than one is well known and several models describing the impact of confinement have been developed. Faksen [10] has obtained a solution in the case where a sphere moves parallel to two plane walls, applying a correction, K_{walls}, to Stokes' law. This correction depends on the position of the sphere, x, relatively to the walls as presented in Figure 2.

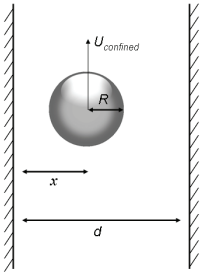

Figure 2. Motion of a sphere parallel to two plane walls.

As a first approximation, it is assumed that the grains nucleate and move along the sample centre line, $x=d/2$. In this case, the corrected velocity as described by Fasken [10] can be expressed as

$$U_{confined} = \frac{U_t}{K_{walls}} = \frac{U_t}{1+1.004\left(\frac{2R}{d}\right)} \tag{4}$$

where R is the radius of the sphere, d is the width of the gap and $U_{confined}$ is the velocity due to confinement.

Results and discussion

As presented above, the model describes the grains which nucleate in the centre of the container and move along the sample centre during buoyant motion. Therefore only a limited number of grains during their early stages of growth will be suitable for comparison with the model. Overall, only 27 grains of the 207 grains selected from the image sequences grew under these conditions. For each composition the average measured velocity, U was compared with U_t, and $U_{confined}$, and the results are shown in Figure 3. The two velocities, U_t and $U_{confined}$ were calculated with the measured average radius, R, as defined above.

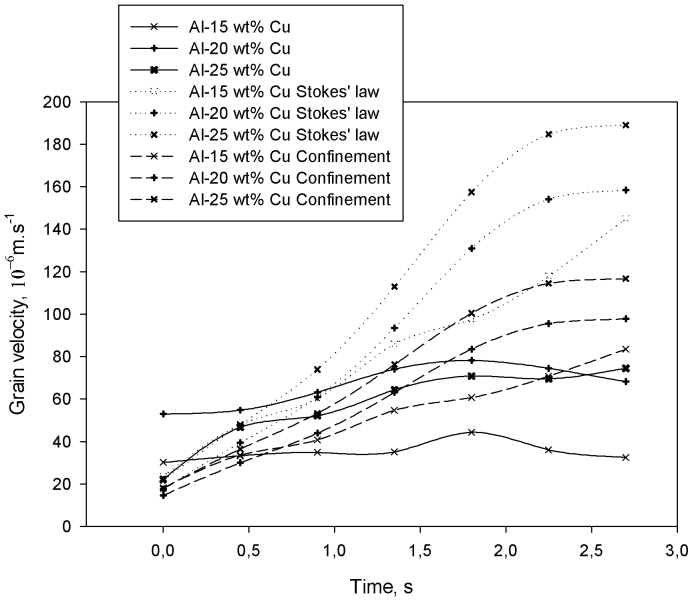

Figure 3. Evolution of the measured grain velocity, U, for the different compositions: 15, 20 and 25 wt% Cu compared with the Stokes' law, U_t and the velocity due to confinement, $U_{confined}$.

The results show that when confinement is considered, the velocity predicted is similar to the measured results, suggesting that confinement is significantly affecting the grain velocity. As the model depends on the measured grain radius, some fluctuations in the velocity calculations appear. Generally, U is lower than $U_{confined}$ especially when time increases, that is when the grain approaches the solidification front.

A simulation of the full sample using FLUENT 6, rules out the presence of any macroscopic fluid flow induced by a combination of confinement and heat transfer over the relevant ranges in G, dT/dt and C_0. In fact, the convection calculated inside the container is most significant at the solidification front where the fluid velocity obtains a maximum velocity of 1 10^{-6}ms^{-1} which can not explain the difference observed in Figure 3. However, the geometry of the mushy zone, the presence of several grains and rejected solute may affect the flow locally. In addition, the assumption that the grain moves along the sample centre during motion may also have to be revised, as fluid flow will influence its position, x during the buoyant transport and thus, K_{walls} in equation (4) will vary. Therefore, as the grain approaches the solidification front these parameters have to be considered and evaluated.

Conclusions

In-situ investigations of equiaxed dendritic growth in grain refined Al–Cu alloys with nominal compositions 15, 20, 25 wt% Cu were carried out at ESRF. Nucleation temperatures, growth rates and velocities due to buoyancy forces on single grains were determined directly from the experiments. The Reynolds number shows that the main forces exerted upon the grain during motion are the buoyant and the drag forces. As the samples are concealed in a thin container, a higher drag force due to the confinement was present resulting in lower velocity, especially when the grain size approaches the sample thickness. A model was developed, allowing the velocity to be determined for grains which nucleate in the centre of the container and move freely through the melt. However, as the grains approach the solidification front, others parameters like mush permeability, geometry of the solid-liquid interface, rejected solute transport and the presence of other equiaxed grains have to be evaluated to improve the model.

REFERENCES

1. L. Arnberg and R.H. Mathiesen, "The Real-Time, High-Resolution X-Ray Video Microscopy of Solidification in Aluminum Alloys," *JOM*, 59 (8) (2007), 20–26.

2. N. Mangelinck-Noël, H. Nguyen-Thi, G. Reinhart, T. Schenk, V. Cristiglio, M.-D. Dupouy, J. Gastaldi, B. Billia, J. Härtwig and J. Baruchel, "In situ analysis of equiaxed growth of aluminium–nickel alloys by x-ray radiography at ESRF," *Journal of physics D: applied physics*, 38 (2005), A28–A32.

3. G. Reinhart, N. Mangelinck-Noël, H. Nguyen-Thi, T. Schenk, J. Gastaldi, B. Billia, P. Pino, J. Härtwig and J. Baruchel, "Investigation of columnar–equiaxed transition and equiaxed growth of aluminium based alloys by X-ray radiography," *Materials Science and Engineering A* 413–414 (2005), 384–388.

4. R.H. Mathiesen, L. Arnberg, K. Ramsøskar, T. Weitkamp, C. Rau and A. Snigirev, "Time-resolved x-ray imaging of aluminium alloy solidification processes," *Metallurgical and Materials Transactions B*, 33B (2002), 613–623.

5. G.Thomas and M.J. Whelan, *Phil. Mag.*, 6 (1961), 1103.

6. J.-H. Lee, S. Liu, H. Miyahara and R. Trivedi, "Diffusion-Coefficient Measurements in Liquid Metallic Alloys," *Metallurgical and materials transactions B*, 35B (2004), 909.

7. S. Ganesan and D.R. Poirier, "Densities of aluminium-rich aluminium-copper alloys during solidification," *Metallurgical Transactions*, A(18) (1987), 721–723.

8. R.F. Brooks, A.T. Dinsdale and P.N. Quested, "The measurement of viscosity of alloys—a review of methods, data and models," *Measurement science and technology*, 16 (2005), 354–362

9. H. Esaka, T. Wakabayashi, K. Shinozuka and M. Tamura, "Origin of Equiaxed Grains and their Motion in the Liquid Phase," *ISIJ International*, 43 (2003), 1415.

10. E.R. Lindgren, "The Motion of a Sphere in an Incompressible Viscous Fluid at Reynolds Numbers Considerably Less Than One," *Physica Scripta*, 60 (1999), 97.